JOURNAL OF SOLID STATE CHEMISTRY 104, 99–118 (1993)

Phase Equilibria and Crystal Chemistry of the Binary and Ternary Barium Polytitanates and Crystallography of the Barium Zinc Polytitanates

R. S. ROTH, C. J. RAWN, C. G. LINDSAY AND W. WONG-NG

Ceramics Division, National Institute of Standards and Technology, Gaithersburg, Maryland 20899

Received October 29, 1992; accepted November 9, 1992

The ternary system BaO–ZnO–TiO_2 is of great interest for use in the production of microwave dielectric ceramics, as the temperature coefficient of the dielectric constant for a ternary phase in the system has the opposite sign from that of the major component in such devices, $BaTi_4O_9$. The ternary system has been found to contain four ternary phases, ideally $BaZn_2Ti_4O_{11}$, $Ba_4ZnTi_{11}O_{27}$, $Ba_2ZnTi_5O_{13}$, and $Ba_xZn_xTi_{8-x}O_{16}$–hollandite. Compatibility triangles for the ternary system have been established and the crystal chemistry and crystal structure of each of the phases was investigated. The phase equilibria data and crystal structures are compared with those encountered in the binary system and other ternary and more complex systems involving barium polytitanates.

1. Introduction

Commercial devices in the microwave industry often use barium polytitanates, $BaTi_4O_9$ and $Ba_2Ti_9O_{20}$, as the major constituents in high frequency dielectric ceramics. Other phases often utilized are $ZrTiO_4$: SnO_2 and $Ba_{3+x}Sm_{4-(2/3)x}Ti_9O_{27}$ (*1*) ($0 \leq x \leq 1$). These ceramics are used in applications requiring a high dielectric constant, *very* low dielectric loss (high Q) at very high frequencies, and a near zero temperature coefficient of the dielectric constant. Unfortunately the barium polytitanates with high dielectric constants and high Q, $BaTi_4O_9$ (1 : 4) and $Ba_2Ti_9O_{20}$ (2 : 9), have a negative temperature coefficient for the dependence of the dielectric constant. Recent devices on the international market utilize ZnO as an additive to counterbalance the negative temperature coefficient (along with other chemical constituents to insure low loss at high frequency). This is partially based on a report that a phase identified as $3BaO \cdot 12TiO_2 \cdot 7ZnO$ has a positive temperature coefficient (*2*). As dielectric properties for coexisting phases are essentially additive, the presence of secondary phases can be used to modify the properties of a given major constituent. Unfortunately the phase equilibria and crystallographic data given in the original report (*2*) could not be verified, so this study was initiated to help verify the real nature of the phases which might be encountered in the system when ZnO is added to barium polytitanates.

2. Binary System Phase Equilibria

2.1. BaO–ZnO

Although no phase equilibrium diagram has been previously published for the sys-

0022-4596/93 $5.00

tem BaO–ZnO, the compound $BaZnO_2$ has been previously reported (*3*). The crystal structure of this phase was deduced from powder data as a "stuffed" β-quartz type and has a hexagonal unit cell, $a = 5.8908$, $c = 6.7362$ Å. This system is currently being examined in detail and will be reported in a future publication (*4*). However, no other compound has been detected in the binary system and as the equilibria in this binary do not affect the data for the polytitanate-type phases it will not be further reviewed in the present publication.

2.2. $ZnO–TiO_2$

Phase equilibria in the $ZnO–TiO_2$ system were reported by Dulin and Rase (*5*), and reproduced as Figure 303 in Phase Diagrams for Ceramists (PDFC) (*6*). Only the spinel-type phase Zn_2TiO_4 (*7*) is stable at high temperature, as $ZnTiO_3$ apparently has a maximum stability temperature of about 945°C.

2.3. $BaO–TiO_2$

2.3.1. Phase Equilibria

The binary system $BaO–TiO_2$ has been extensively studied because of the many useful properties of its compounds. It was first described by Rase and Roy (*8*) (PDFC 213) as containing Ba_2TiO_4 (2 : 1), $BaTiO_3$ (1 : 1) with both cubic or tetragonal and hexagonal polymorphs, $BaTi_2O_5$ (1 : 2), $BaTi_3O_7$ (1 : 3), and $BaTi_4O_9$ (1 : 4). Negas *et al.* (*9*) (PDFC 4302) showed that $BaTi_2O_5$ did not exist at temperatures between 1200°C and the solidus, ~1320°; that the compound $BaTi_3O_7$ ("1 : 3") did not exist but was made up of two phases having the compositions $Ba_6Ti_{17}O_{40}$ (6 : 17) and $Ba_4Ti_{13}O_{30}$ (4 : 13); and that another phase $Ba_2Ti_9O_{20}$ (2 : 9) was also stable between ~1200–1300°C. Roth and co-workers (*10*) using amorphous precursor ethoxide specimens found that $BaTi_2O_4$ was stable at low temperatures but decomposed at a temperature slightly above 1100°C, although it was easily prepared by quenching the eutectic liquid near this composition. In addition the compound $BaTi_5O_{11}$ (1 : 5) was also found to be stable at low temperatures but decomposed at about 1200°C. O'Bryan and Thompson (*11*), PDFC 5135, refined the melting points of the polytitanates and in the latest version Kirby and Wechsler (*12*) have again slightly modified the melting points and emphasized that only 6 : 17, 4 : 13, 1 : 4, and 2 : 9 are stable above 1250°C. The phase "$Ba_2Ti_5O_{12}$" (2 : 5) which had been reported to be stabilized by isovalent SnO_2 or ZrO_2 substitution (*13*) was found to occur at very low temperature in the pure ethoxide precursor but to be stable at high temperature only with the addition of ZrO_2 (*14*).

2.3.2. Crystal Structure

The unit cell dimensions of the barium polytitanates (*15*) as well as the ternary polytitanates are shown in Table I. The crystal structures of the barium polytitanates have been very extensively studied. As the dielectric properties of ceramics are strongly structure dependent, it is of interest to thoroughly understand these structures in an attempt to learn how to fine-tune the necessary properties for different applications.

The various polytitanates can be classified into two structure types: (1) anions in mixed "cubic" packing, with regions of corner-sharing octahedra in an ReO_3-like array (anions in approximately face-centered cubic packing) and regions of edge-sharing octahedra (anions in approximately body-centered cubic packing); the occupied octahedra form double layers perpendicular to 4-fold axes of the octahedra and share edges between the two levels of this layer and corners or edges within one level (see Fig. 1a). (2) anions and Ba^{2+} cations in (approximate) hexagonal closest-packing, with occupied octahedra forming discontinuous layers per-

TABLE I

UNIT CELL DIMENSIONS OF THE BINARY AND TERNARY POLYTITANATES

Notation phase	Symmetry and space group	a	b	c	α	β	γ	Number of layers	References
				Cubic Packing					
1 : 2	monoc								
$BaTi_2O_5$	$C2/m$	16.914(1)	3.9345(3)	9.4122(7)	—	103.114(6)	—	—	(*15–17*)
1 : 4	ortho								
$BaTi_4O_9$	$Pnmm$	6.2940(5)	14.5324(1)	3.7972	—	—	—	—	(*15, 18, 19*)
2 : 1 : 5	monoc								
$Ba_2MgTi_5O_{13}$	$C2/m$	15.208	3.899	9.109	—	98.5	—	—	(*31*)
$Ba_2ZnTi_5O_{13}$	$C2/m$	15.235	3.8416	9.117	—	98.5	—	—	present work
				Hexagonal Packing					
6 : 17	monoc								
$Ba_6Ti_{17}O_{40}$	$C2/m$	9.890(1)	17.117(2)	18.933(2)	—	98.71(1)	—	8	(*9, 15, 20*)
4 : 13	ortho								
$Ba_4Ti_{13}O_{30}$	$Cmca$	17.072(2)	9.862(1)	14.059(1)	—	—	—	6	(*9, 15, 21*)
2 : 9	tricl								
$Ba_2Ti_9O_{20}$	$P\bar{1}$	7.471	14.081	14.344	89.94	79.43	84.45	6	(*22, 26*)
1 : 5	monoc								
$BaTi_5O_{11}$	$P2_1/n$	7.6691(4)	14.0410(8)	7.5335(5)	—	98.359(5)	—	6	(*15, 23, 25*)
1 : 6	tricl								
$BaTi_6O_{13}$	$P\bar{1}$	7.510(2)	9.852(3)	7.461(2)	105.38(3)	118.90(3)	72.58(3)	4	(*24*)
11 : 28-"2 : 5"	monoc								
$Ba_{11}Ti_{28}O_{66}O$	$C2/m$	23.528	11.482	9.941	—	~90	—	10	(*14*)
4 : 2 : 10	monoc								
$Ba_4Al_2Ti_{10}O_{27}$	$C2/m$	19.737	11.349	9.837	—	109.4	—	8	(*32*)
4 : 1 : 11	monoc								
$Ba_4ZnTi_{11}O_{27}$	$C2/m$	19.898	11.467	9.915	—	109.5	—	8	present work
6 : 2 : 14	orth								
$Ba_6Nb_2Ti_{14}O_{39}$	$Cmc2_1$	17.138	9.868	18.759	—	—	—	8	(*35*)
10 : 2 : 28	monoc								
$Ba_{10}Nb_2Ti_{28}O_{72}$	$C2/m$	~9.87	~17.14	16.72	—	101.2	—	7	(*35*)
9 : 1 : 27	monoc								
$Ba_9NbTi_{27}O_{66}$	$C2/m$	~9.87	~19.14	~30.65	—	~96	—	13	(*35*)
14 : 2 : 40	orth								
$Ba_{14}Nb_2Ti_{40}O_{99}$	Cmc^*	~17.14	~9.87	~46.86	—	—	—	20	(*35*)
1 : 2 : 4	orth								
$BaZn_2Ti_4O_{11}$	$Pnab$	10.1189(5)	11.5906(6)	14.1338(7)	—	—	—	—	present work

pendicular to three-fold axes of the octahedra; the octahedra are either isolated or share edges within a layer (see Fig. 1b). Occasionally, occupied octahedra in adjacent layers can share a face.

The ideal structure of such polytitanates can then be described by the number of such layers in the unit cell and the distribution of Ba^{2+} and Ti^{4+} ions within these layers.

The patterns drawn by all these structures are dictated by the A-cation : B-cation : anion ratios and by the crystallographic symmetry. The octahedrally coordinated Ti^{4+} ions always form an "aesthetically pleasing" pattern and the thermodynamically more stable phases adopt the higher

FIG. 1. Representation of Ti and (Ti, *Me*) octahedra for (a) Body centered cubic packing of anions. The darker octahedra are in the upper level of a two-level layer. (b) Hexagonal close packing of anions, showing corner and edge sharing of octahedra.

symmetry orthorhombic structures. Each structure is unique to a given stoichiometric compound and gross deviations from stoichiometry result in formation of a second phase. Introduction of more than a few parts per million of aliovalent ions results in the formation of a second phase, or an extended defect usually detectable by high resolution electron microscopy (HREM) lattice imaging.

2.3.2.1. Cubic packing. Two of the barium polytitanates have structures which can be described as based on cubic packing of anions, with Ba ions occurring at the same levels as the oxygens. The crystal structures of $BaTi_2O_5$ and $BaTi_4O_9$ are shown in Figs. 2 and 3 in ideal form. The atomic positions in the refined structures published for each of these phases, (*16, 17*) for 1 : 2 and (*18, 19*) for 1 : 4, deviate only slightly from the ideal positions.

2.3.2.2. Hexagonal packing. The structures of the other polytitanates are more complex, but can be illustrated as made up of hexagonal close packed layers with 4–6–8–10 layers per unit cell. Each of the orthorhombic and monoclinic compounds has one dimension of ~17 Å or ~10 Å and the other of about 9 Å. The unit cells are either 6 octahedra wide (~17 Å) or 4 octahedra wide (~10 Å) and generally 4 octahedra long (~9.8 Å). For the ~17 Å-type unit cell each close-packed layer contains 6 × 4 = 24 hexagonal intersection nodes. Thus, for each layer, the sum of Ba^{2+} + O^{2-} + vacancy = 24. A vacancy can *only* occur if two Ba ions substitute for three oxygens in a row, leaving the vacancy between the two barium ions. For the ~10 Å cell the sum of the Ba^{2+} + O^{2-} + vacancy = 4 × 4 = 16. The number of hexagonally packed layers is a multiple of the thickness of a layer, ~2.3Å, times 4, 6, 8, 10 (or sometimes even an odd number for some ternary phases). The crystal structure of each of the polytitanates is shown in ideal form, in Figs. 4–8. $Ba_6Ti_{17}O_{40}$ (6 : 17) (*9, 20*), Fig. 4, is an eight layer phase with monoclinic symmetry while $Ba_4Ti_{13}O_{30}$ (4 : 13) (*9, 21*) is an orthorhombic six layer phase with a very similar but more symmetrical distribution of titanium octahedra in the layers. In fact the 4 : 13 phase and its structure, Fig. 5, were predicted by Negas *et al.*(*9*) based on the published structure of the 6 : 17 phase (*20*), without previous knowledge of its existence. The structures of $Ba_2Ti_9O_{20}$ (2 : 9) (*22*), Fig. 6, and $BaTi_5O_{11}$ (1 : 5) (*23*), Fig. 7, also obey these cation/cation/anion ratios. The 2 : 9 phase is triclinic with a unit cell 6 octahedra wide but only 3 octadedra long, while 1 : 5 has monoclinic symmetry and with a unit cell (~7.5A) only ~3 octahedra wide and long. Another triclinic structure, Fig. 8, has been

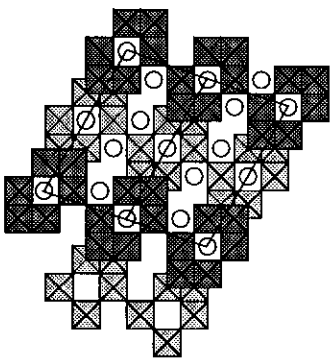

FIG. 2. Ideal representation of the crystal structure of $BaTi_2O_5$, after (*16,17*). As in Fig. 1a the darker octahedra are in the upper level.

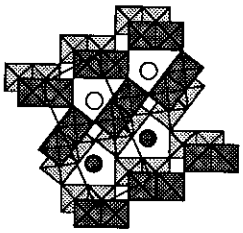

FIG. 3. Ideal representation of the crystal structure of $BaTi_4O_9$, after (*18, 19*). As in Fig. 1a the darker octahedra are in the upper level.

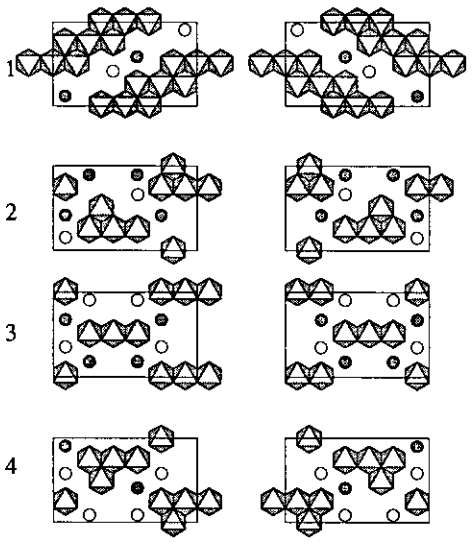

FIG. 4. Ideal representation of the crystal structure of $Ba_6Ti_{17}O_{40}$ at the eight Ti levels in the unit cell, after (*19, 20*). In this and all subsequent structure diagrams of Ba-containing phases, the dark and light circles represent Ba atoms at the oxygen levels above and below the metal atoms respectively.

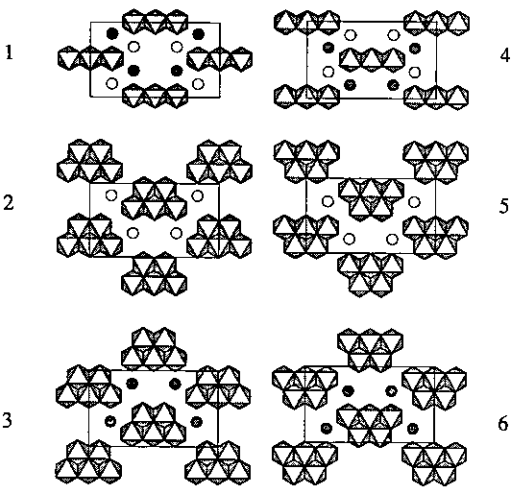

FIG. 5. Ideal representation of the crystal structure of $Ba_4Ti_{13}O_{30}$ at the six Ti levels in the unit cell, after (*19, 20*).

reported for a metastable crystal obtained only from a melt with the composition $BaTi_6O_{13}$ (1 : 6) (*24*) and its unit cell is also only ~3 octahedra wide. These compounds often exhibit extended defects which generally accommodate the same composition as the original (*25, 26*). Although theoretically such defects *could* account for nonstoichiometry as found for the cubic packing of the Nb_2O_5–WO_3 phases (*27, 28*), no

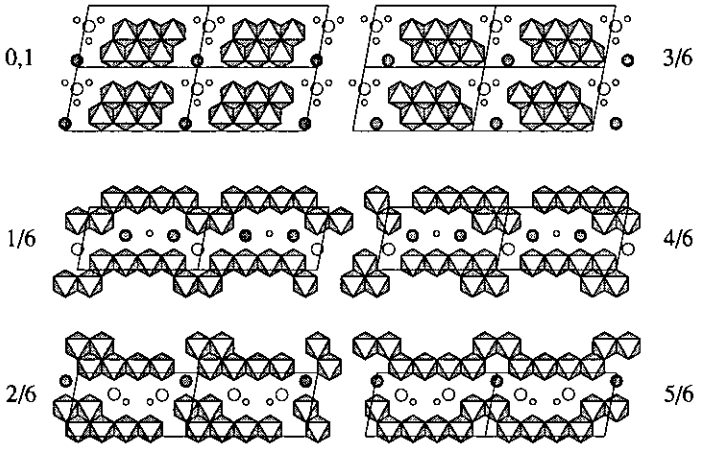

FIG. 6. Ideal representation of the crystal structure of $Ba_2Ti_{13}O_{30}$ at the six Ti levels in the unit cell. Large circles are Ba and small circles are oxygen not coordinated to a Ti atom at the level indicated, after (*22a,b, 26*).

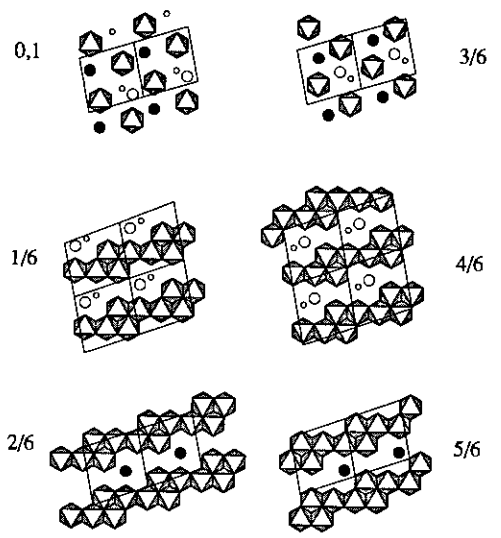

FIG. 7. Ideal representation of the crystal structure of $BaTi_5O_{11}$ at the six Ti levels in the unit cell, after (*23, 25, 42*).

such defects have been reported in the $BaO–TiO_2$ phases.

3. Ternary Systems

3.1. $BaO–TiO_2–ZrO_2$

The ternary systems $BaO–TiO_2–ZrO_2$ and $BaO–TiO_2–SnO_2$ were reported by Jonker and Kwestroo (*13*) long before it was realized that the "1 : 3" phase did not exist. However, both systems were reported to contain the 2 : 5 phase which was not known for the binary system. In an attempt to define the stability of the 2 : 5 compound, Roth *et al.* (*14*) noted that it only occurred at temperatures below ~650° for ethoxide precursors in the binary system; it was stable at high temperature only in the ZrO_2 system and not in the SnO_2 system. A phase equilibrium diagram of the $BaO–TiO_2–ZrO_2$ system after (*13*) but revised to obey the currently known equilibria (*14, 29*) is given in Fig. 9. A crystal of the "2 : 5" phase was used in (*14*) to establish that the structure is that of an eight-layer ~10 Å hexagonally packed type with monoclinic symmetry (mistakenly labeled triclinic in (*14*)). The ideal structure of this phase is shown in Fig. 10 from as yet unpublished data of Gatehouse *et al.* (*30*). Its structure turns out to contain 11 Ba^{2+} to 28 Ti^{4+} ions (2 : 5 = 28.57 mole percent BaO while 11 : 28 = 28.205 mole percent BaO) and 66 instead of 67 oxygen ions, $Ba_{11}Ti_{28}O_{66}O$. Either the phase is stablized by some trivalent impurity (Al^{3+}) or an extra oxygen may be partially filling the site marked as a vacancy in Fig. 10. Reduction of some of the Ti^{4+} to Ti^{3+} is not a likely explanation as the phase is white/transparent not black or dark grey.

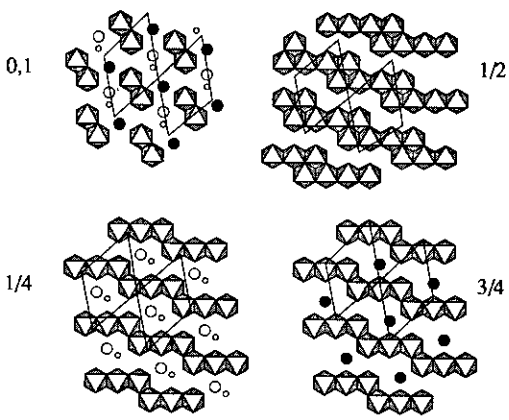

FIG. 8. Ideal representation of the crystal structure of $BaTi_6O_{13}$ at the four Ti levels in the unit cell, after (*24, 25*).

3.2. $BaO–TiO_2–Al_2O_3$

The ternary system $BaO–TiO_2–Al_2O_3$ contains several ternary phases and the previously reported diagram (*31*) PDFC 6643 is reproduced here as Fig. 11. This system contains a nonstoichiometric solid solution with the hollandite structure and the formula $Ba_xAl_{x/2}Ti_{8-x/2}O_{16}$ ($1.14 \leq x \leq 1.23$). The nonstoichiometric hollandite phase is known to be detrimental to high Q (low loss) microwave dielectric properties. Another phase, $Ba_4Al_2Ti_{10}O_{27}$ (4 : 2 : 10), belongs to the ~10 Å hexagonally packed series. The

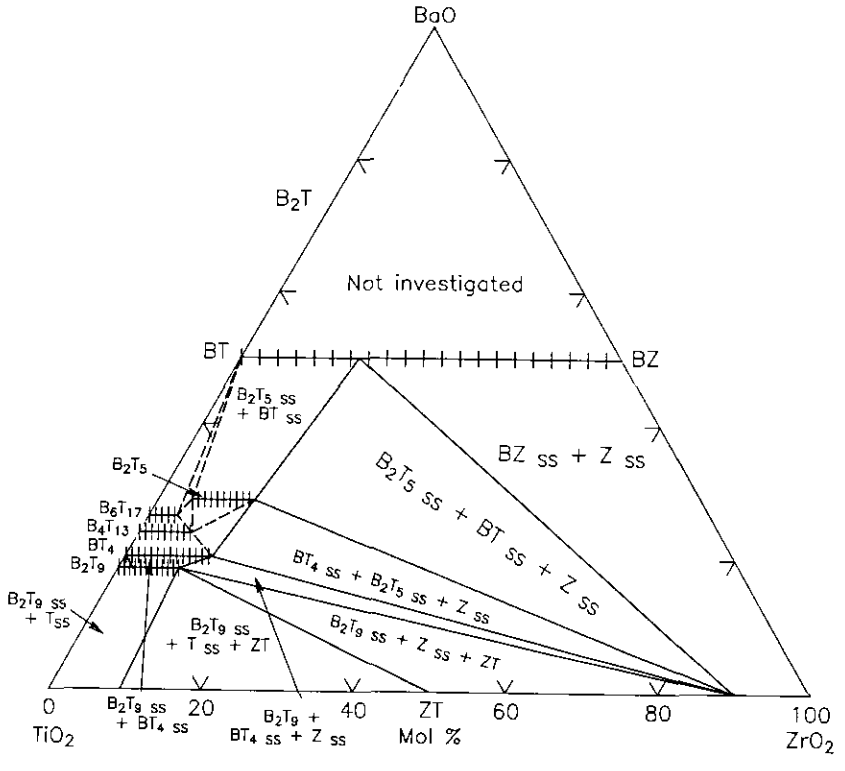

FIG. 9. Phase equilibria diagram of the system $BaO–TiO_2–ZrO_2$, modified from (*13*, *29*).

ideal structure is shown in Fig. 12 based on the crystal structure published by Schmachtel and Müller-Buschbaum (*32*). Note that this composition differs from that of "$BaTi_3O_7$" by $\frac{1}{4}$ of an oxygen atom and indeed the reduced phase $Ba_4Ti_2^{3+}Ti_{10}^{4+}O_{27}$ was reported to exist (*32*).

3.3. $BaO–TiO_2–MgO$

The system $BaO–TiO_2–MgO$ was also previously reported in (*31*) and as PDFC 6632. This system also contains the nonstoichiometric hollandite phase $Ba_xMg_xTi_{8-x}O_{16}$ as well as two other ternary phases. One of these represents the phase $BaMg_6Ti_6O_{19}$ and because of its hexagonal structure was named barium hexageikielite in analogy to barium hexaferrite and "barium hexaluminate". The other compound was mistakenly assigned the compositon BaMg Ti_3O_8 (1 : 1 : 3). However, the unit cell dimensions of this phase and additional experimental data in the present system indicate that the composition is really $Ba_2MgTi_5O_{13}$ (2 : 1 : 5) and is isostructural with potassium hexatitanate $K_2Ti_6O_{13}$ (*33*). The revised phase diagram is given in Fig. 13.

3.4. $BaO–TiO_2–Nb_2O_5$

The system $BaO–TiO_2–Nb_2O_5$ contains a large number of ternary phases (*34*, *35*). Those phases which belong to the ternary hexagonally packed polytitanates are described (*35*) in Fig. 14. The most stable of these polytitanates is an 8-layer orthorhombic phase $Ba_6Nb_2Ti_{14}O_{39}$. The ideal structure based on space group $Cmc2_1$ rather than *Cmca* is shown in Fig. 15 from data obtained

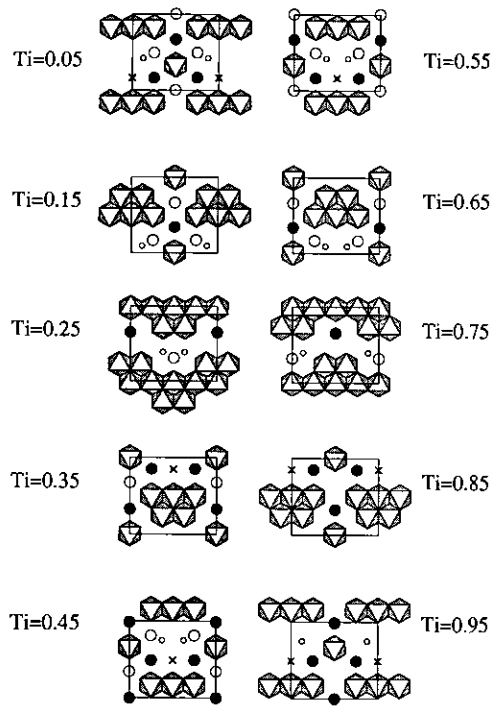

FIG. 10. Ideal representation of the crystal structure of the phase originally designated as $Ba_2Ti_5O_{13}$ (*13, 14*). The crystal structure refinement (*30*) indicates that the true formula is $Ba_{11}Ti_{28}O_{66}$ with the 67th oxygen ion possibly in any of the vacancy positions denoted by *X*.

from single crystals (*30*). At least three other polytitanates have been isolated in this system. Although their exact compositions and structures have not been refined by single crystal structure determination, the proposed compositions, symmetries and number of layers were determined from isolated crystals (*35*). These phases are a 7-layer monoclinic phase, $Ba_{10}Nb_2Ti_{28}O_{72}$; a 20-layer orthorhombic (*Cmc**) phase, $Ba_{14}Nb_2Ti_{40}O_{99}$; and a 13-layer monoclinic phase, $Ba_9NbTi_{27}O_{66}$. All these barium niobium polytitanates have the 6-octahedra wide (~17 Å) type unit cell.

3.5. $BaO–TiO_2–ZnO$

Phase equilibria in the system $BaO–TiO_2–ZnO$ have not been previously reported. However, the system $BaTi_4O_9$ (1 : 4)–ZnO was studied (*2*). It was stated that about 5 wt% zinc oxide went into solid solution in $BaTi_4O_9$ and a second phase occurred whose composition was stated to be $Ba_3Ti_{12}Zn_7O_{34}$. It was pointed out that this phase had the opposite sign to the temperature coefficient of the dielectric constant (positive) and therefore could be used to compensate the negative coefficient in ceramic specimens of $BaTi_4O_9$. The compound was said to be orthorhombic with a = 6.390, b = 6.875, c = 7.045 Å and a partially indexed X-ray pattern was published. Unfortunately, these numbers are incorrect and fail to adequately index the reported pattern.

About 35 specimens were prepared by solid state reaction and heat treated as pellets, first at 1000°C and then at 1250°C on Pt foil. All specimens were mixed and ground together from $BaCO_3$, 99.99% TiO_2 (with no P_2O_5 or SiO_2 as impurities) and ZnO. Some of the specimens were again treated at 1350°C to see if equilibrium conditions changed. Specimens were often given second or even more heat treatments at a given temperature to ensure equilibrium. In portions of the system where melting was suspected to occur between 1250 and 1350°C specimens were heated and quenched in a vertical tube furnace in sealed or unsealed Pt tube containers. All furnaces were calibrated at the melting point of Au, 1063°C.

The phase equilibrium diagram derived from the data obtained from X-ray diffraction powder patterns of the prepared specimens is shown in Fig. 16 and an enlarged version of the high TiO_2 corner is shown in Fig. 17. $BaTiO_3$ apparently accepts less than about 2 mol% ZnO in solid solution. No solid solution of ZnO in any of the binary barium polytitanates was observed. The system contains at least four ternary phases. The ternary phases shown in Figs. 16 and 17 which are stable at 1250°C are (1) $Ba_xZn_xTi_{8-x}O_{16}$ with the hollandite structure, (2)

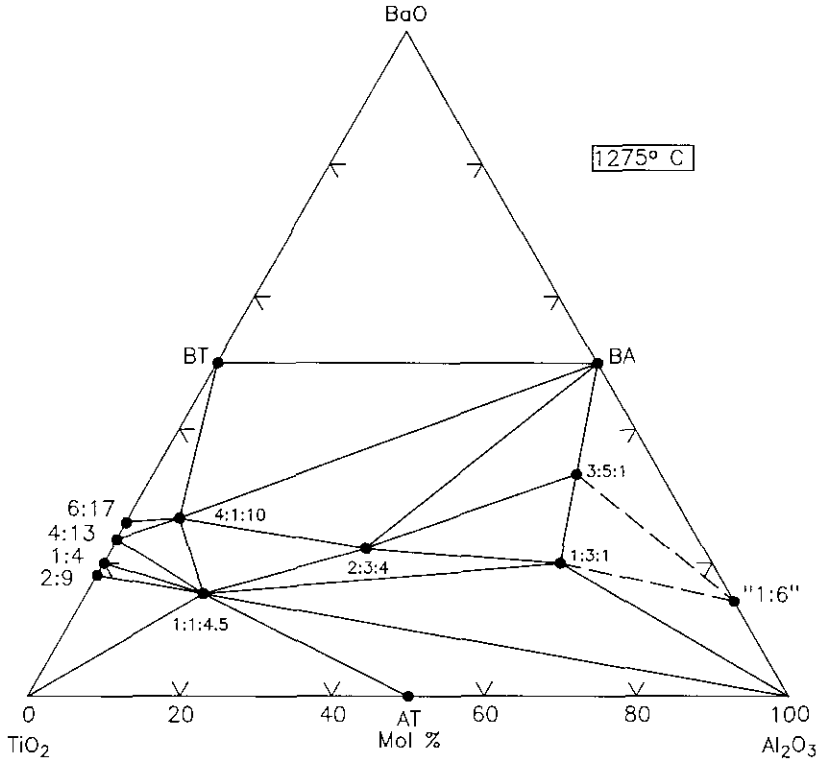

FIG. 11. Phase equilibria diagram of the system $BaO–TiO_2–Al_2O_3$ from (*31*), PDFC 6643A.

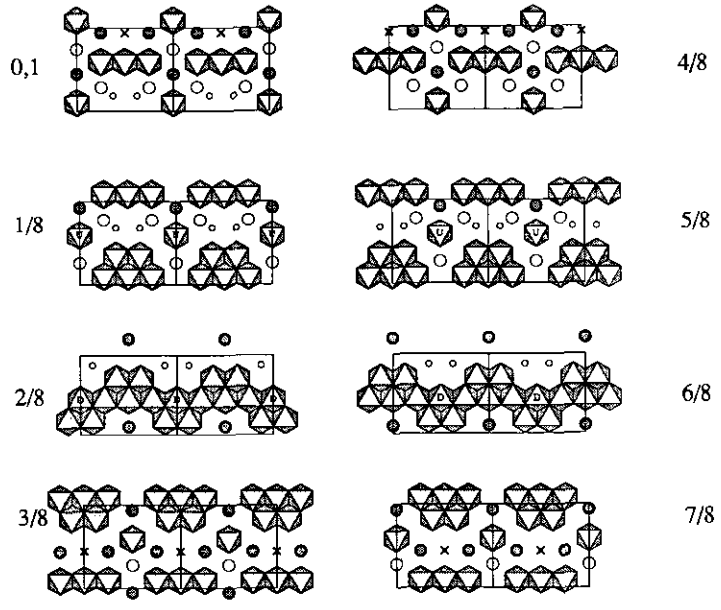

FIG. 12. Ideal representation of the crystal structure of $Ba_4Al_2Ti_{10}O_{27}$, after (*32*). The phases Ba_4Mg $Ti_{11}O_{27}$ and $Ba_4ZnTi_{11}O_{27}$ are apparently isostructural. U and D indicate octahedra that share faces with another octahedron above or below, respectively.

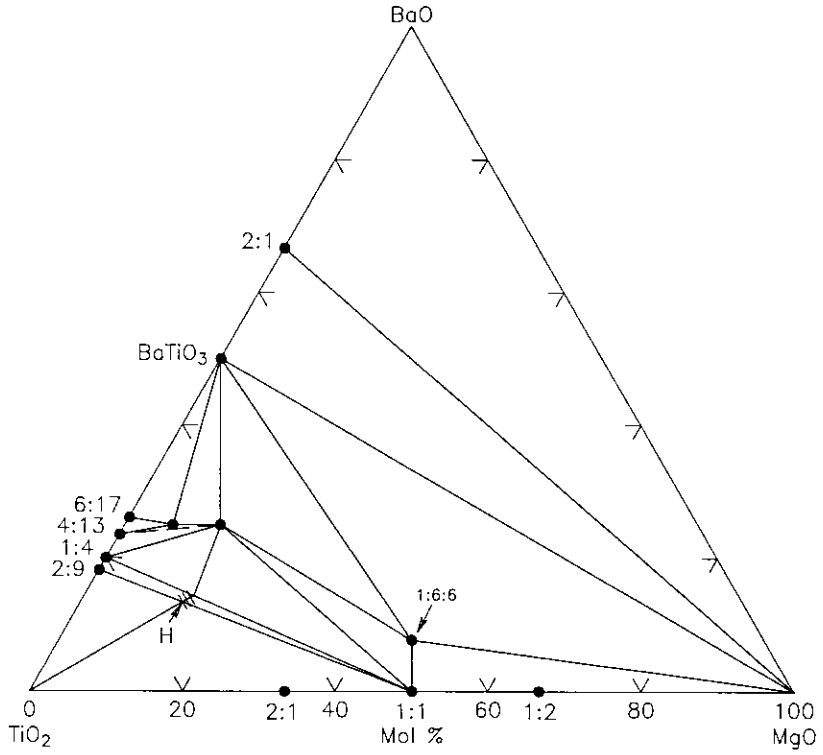

FIG. 13. Phase equilibrium diagram of the system $BaO–TiO_2–MgO$ modified from (*31*), showing the two newly located compounds $Ba_4MgTi_{11}O_{27}$ and $Ba_2MgTi_5O_{13}$.

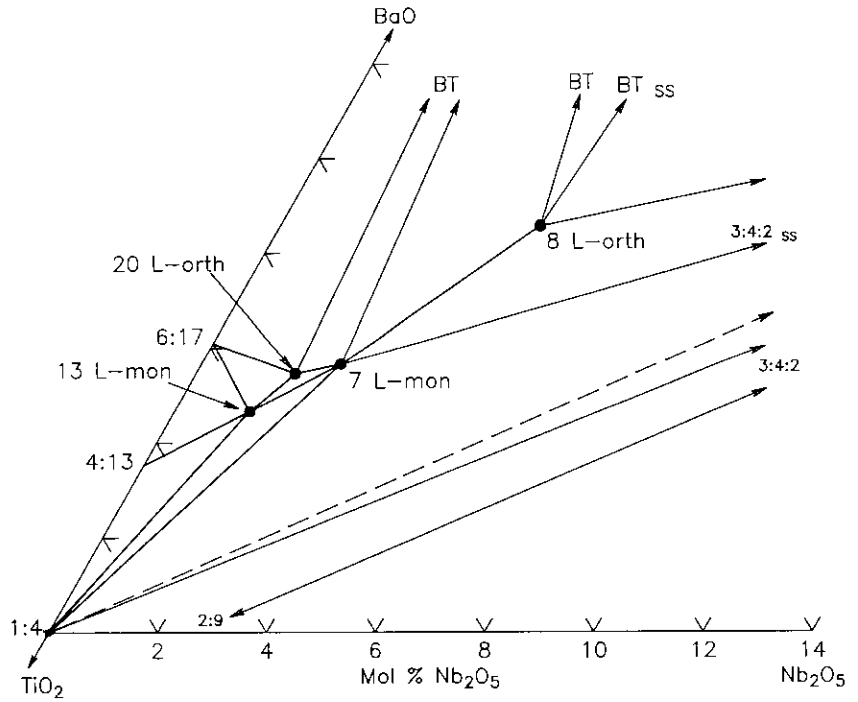

FIG. 14. Enlarged portion of the polytitanate region of the phase equilibria diagram of the system $BaO–TiO_2–Nb_2O_5$ from (*35*).

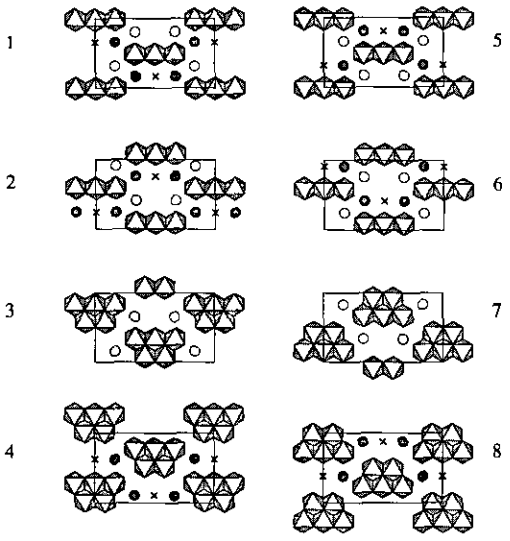

FIG. 15. Ideal representation of the crystal structure of $Ba_6Ti_{14}Nb_2O_{39}$ at the eight (Ti, Nb) levels in the unit cell, after (*30*). Vacancies are denoted by *X*.

$Ba_4ZnTi_{11}O_{27}$—isostructural with $Ba_4Al_2Ti_{10}O_{27}$, (3) $Ba_2ZnTi_5O_{13}$—apparently isostructural with potassium hexatitanate, $K_2Ti_6O_{13}$, and $Ba_2MgTi_5O_{13}$, and (4) $BaZn_2Ti_4O_{11}$ or $Ba_3Zn_6Ti_{12}O_{33}$ rather than the previously reported composition $Ba_3Zn_7Ti_{12}O_{34}$, which has a unique structure, as reported below. Single crystals of each of these phases were grown by heating appropriate compositions in sealed Pt tubes above about 1400°C and slow cooling, generally at 3°C/hr to 1250°C. Single crystals were picked from the cooled melts and examined by single crystal X-ray precession patterns to establish the symmetry, unit cells, and space groups and unit cells as shown in Table I. This technique proved that the previously reported phase was orthorhombic with space group *Pnab* and unit cell dimensions $a = 10.1189(5)$, $b = 11.5906(6)$, $c =$

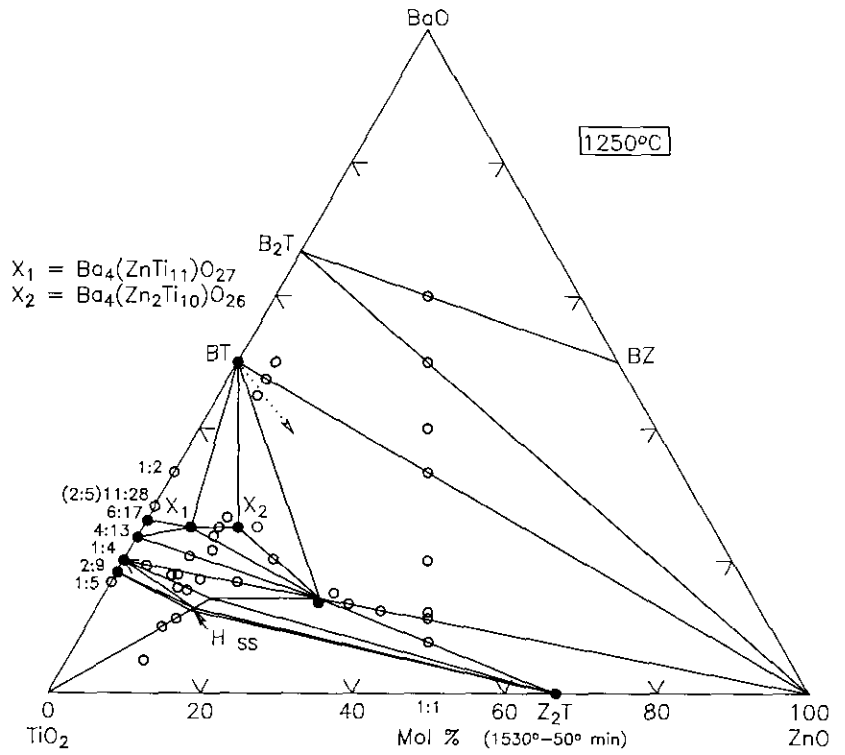

FIG. 16. Phase equilibria diagram of the system BaO–TiO_2–ZnO. Filled circles represent compounds stable at 1250°. Open circles represent compositions of most of the specimens prepared for the study. Dotted arrow represents the apparent direction of the maximum amount of solid solution of ZnO in $BaTiO_3$.

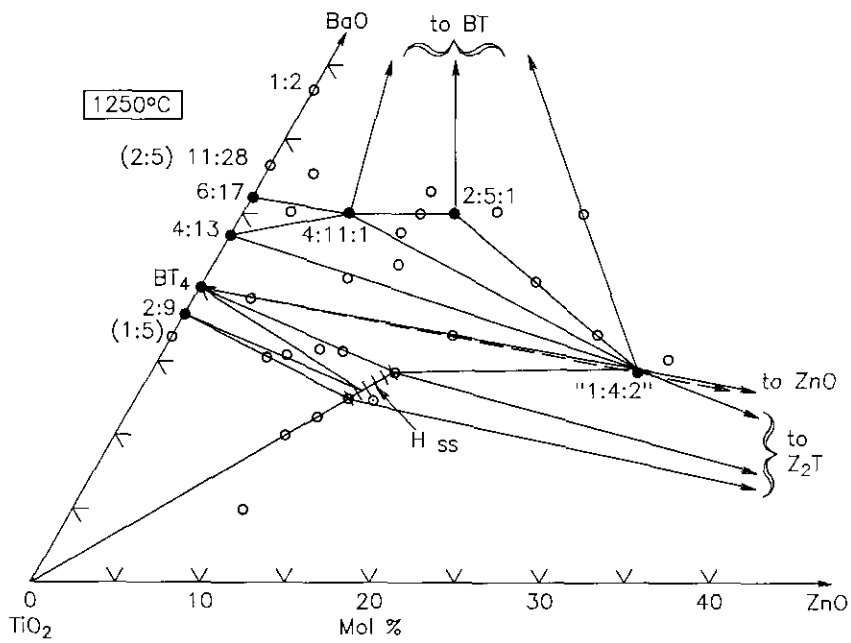

FIG. 17. Enlarged portion of Fig. 16. Dashed line illustrates the tie line $BaTi_4O_9$–ZnO which apparently lies just below the join for the two phase tie line of $BaTi_4O_9$–"$BaZn_2Ti_4O_{11}$."

14.1338(7) Å, after the powder pattern was refined by least square analyses.

The X-ray powder diffraction patterns of the compositions near $BaO:2ZnO:4TiO_2$ (1:2:4) heated to temperatures of 1000°C and below, always show a phase similar to the one obtained at higher temperatures but enough different that it obviously represents a different phase. Despite numerous attempts to synthesize single crystals of this low temperature form we still do not know its composition or unit cell. The high temperature form does not reverse with repeated heat treatments at 1000°C. Attempts to grow crystals with a flux of barium borate, boric acid, or barium vanadate by slow cooling from 1000°C all results in formation of crystals of the high temperature form. Heating the 1:2:4 composition with boric acid at 900°C results in a slightly more crystalline version of the low temperature phase together with various borate phases but no usable single crystals. Attempts are still underway to determine the composition, unit cell, structure, and stability of this phase and further details will be reported at a later date.

4. Crystal Structure Determination

Among the four ternary phases discussed above, $Ba_2ZnTi_5O_{13}$ and $BaZn_2Ti_4O_{11}$ have been studied using single crystal diffraction techniques. Preliminary examination and data collection for these two compounds were performed on a computer-controlled diffractometer[1] using single crystals previously examined with a precession camera. Cell constants and orientation matrices for

[1] CAD4 Diffractometer, Enraf–Nonius, Inc. Netherlands. This equipment is identified by trade name in this article for complete specification of experimental procedures. Such identification does not imply recommendation or endorsement by the National Institute of Standards and Technology.

data collection were obtained from least squares refinements, using the setting angles of 25 reflections in the range of $10° < \theta < 16°$ for $Ba_2ZnTi_5O_{13}$ and $13° < \theta < 24°$ for $BaZn_2Ti_4O_{11}$. Three standard reflections used for monitoring the stability of the crystal showed negligible variation in intensity. A semiempirical absorption correction was performed by using the psi scan technique (*36*). Lorentz and polarization corrections were applied to both data sets (*36*). The structure solution and refinements were carried out on a VAX computer using the software suite MOLEN (*37*). In both compounds it was found that mutual substitution of atoms, i.e., Zn for Ti and Ti for Zn, probably occurred, indicated by abnormally small or large temperature factors. The disordered atom method (MOLEN) was applied for refinement. In this method, the atomic positions and thermal parameters for the two types of atoms sharing the same site were constrained to be the same. Table II summarizes the experimental and structural solution details. The relatively higher R value for the compound $BaZn_2Ti_4O_{11}$ may be due to incomplete correction for absorption error. Note that the unit cell of this platy crystal is considerably larger than that of $Ba_2ZnTi_5O_{13}$. Tables IIIa and IIIb give the posi-

TABLE II

CRYSTALLOGRAPHIC AND STRUCTURE SOLUTION DETAILS

	$Ba_2ZnTi_5O_{13}$	$BaZn_2Ti_4O_{11}$
Crystal dimensions	0.15 × .005 × 0.13 mm	0.35 × 0.2 × 0.1mm
Crystal system	Monoclinic	Orthorhombic
Space group	*C2/m* (No. 12)	*Pbcn* (No. 60)
Cell parameters		
a	15.236(2)	14.140(3)
b	3.8992(7)	11.592(2)
c	9.139(2)	10.1173(13)
β	98.78(2)	
Z	2	8
Density (calc)	4.87 g/cm^3	5.09 g/cm^3
Mo$K\alpha$ radiation	0.71073 Å	0.71073 Å
Temperature	≈295 K	≈295 K
Monochromator	graphite	graphite
Data range	$0 < h < 22$	$0 < h < 18$
	$-1 < k < 5$	$-15 < k < 2$
	$-13 < l < 13$	$0 < l < 13$
Reflections		
total	1319	2725
unique	1052	2303
Corrections		
absorption	32.9%–99.9% on I	48.9%–99.9% on I
extinction	$\|2.19 \times 10^{-6}\|$	$\|1.03 \times 10^{-7}\|$
Solution	Direct method	Heavy atom method
# Reflections	968 ($I > 3\sigma$)	1719 ($I > 3\sigma$)
Parameters refined	45	100
Function minimized	$\Sigma w(\|F_o\| - \|F_c\|)^2$	$\Sigma w(\|F_o\| - \|F_c\|)^2$
Weight, non-Poisson	$p = 0.04$	$p = 0.04$
Unweighted residual	0.044	0.064
Weighted residual	0.065	0.097
goodness of fit	2.43	2.59

TABLE IIIa

POSITIONAL AND THERMAL PARAMETERS FOR $Ba_2ZnTi_5O_{13}$

Atom	x	y	z	$U(1,1)$	$U(2,2)$	$U(3,3)$	$U(1,2)$	$U(1,3)$	$U(2,3)$
Ba1	0.44973(3)	0.000	0.23209(5)	0.0132(2)	0.0085(2)	0.0166(2)	0	0.0011(2)	0
Ti1[1]	0.66941(8)	0.500	0.4392(1)	0.0075(4)	0.0091(4)	0.0087(4)	0	−0.0001(4)	0
TZ[2]	0.75969(7)	1.000	0.2283(1)	0.0116(4)	0.0105(4)	0.0130(4)	0	0.0034(4)	0
Ti2[3]	0.61909(8)	0.500	0.0939(1)	0.0085(4)	0.0108(4)	0.0097(5)	0	0.0005(4)	0
O1	0.3338(4)	−0.500	0.0851(7)	1.18(8)*					
O2	0.5715(4)	0.500	0.2991(6)	0.94(7)*					
O3	0.500	0.500	0.000	1.5(1)*					
O4	0.3710(4)	−0.500	0.3856(7)	1.32(8)*					
O5	0.7355(4)	0.500	0.2398(6)	0.91(7)*					
O6	0.3684(4)	0.000	−0.1100(6)	1.12(8)*					
O7	0.2992(4)	0.000	0.5682(6)	0.80(7)*					

Note. Site occupancy: [1] *0.475* Ti + *0.025* Zn; [2] *0.2* Zn + *0.3* Ti; [3] *0.475* Ti + *0.025* Zn. Starred atoms were refined isotropically. Anisotropically refined atoms are given in the form of the isotropic equivalent displacement parameter, defined as $\exp[-2\pi\{h^2a^2U(1,1) + k^2b^2U(2,2) + l^2c^2U(3,3) + 2hkabU(1,2) + 2hlacU(1,3) + 2klbcU(2,3)\}]$, where a, b, c are reciprocal lattice constants.

tional and thermal parameters and Tables IVa and IVb give the selected bond distances and angles for $Ba_2ZnTi_5O_{13}$ and $BaZn_2Ti_4O_{11}$, respectively.

4.1. Crystal Structure of $Ba_2ZnTi_5O_{13}$

This compound, which was found to be isostructural with potassium hexatitanate, $K_2Ti_6O_{13}$ (*33*), crystallizes in the form of thin sheets. It has a short b axis (3.9 Å), which corresponds to the axial O–Ti–O distance in a TiO_6 octahedron. The projection of the ideal structure along b is shown in Fig. 18. Figure 19 illustrates the corresponding experimental packing diagram. The overall structure can be described as consisting of

TABLE IIIb

POSITIONAL AND THERMAL PARAMETERS FOR $BaZn_2Ti_4O_{11}$

Atom	x	y	z	$U(1,1)$	$U(2,2)$	$U(3,3)$	$U(1,2)$	$U(1,3)$	$U(2,3)$
Ba	0.09209(4)	0.36639(4)	0.57439(6)	0.0104(3)	0.0121(3)	0.0039(3)	−0.0008(2)	0.0007(2)	0.0002(2)
Zn1	0.04126(8)	0.11882(8)	0.4088(1)	0.0093(6)	0.0091(4)	0.0014(5)	0.0007(4)	0.0000(4)	−0.0005(4)
Zn2	0.3266(1)	0.1075(1)	0.4025(1)	0.0131(6)	0.0163(5)	0.0043(6)	0.0034(5)	0.0027(5)	0.0008(5)
Ti1[1]	0.3227(1)	0.4908(1)	0.1574(2)	0.54(2)*					
Ti2[2]	0.3265(1)	0.3645(1)	0.4157(2)	0.58(3)*					
Ti3[3]	0.1666(1)	0.2596(1)	0.1820(2)	0.0080(7)	0.0107(6)	0.0024(8)	−0.0010(6)	0.0008(7)	−0.0001(6)
Ti4	0.000	0.1367(2)	0.750	0.007(1)	0.0096(6)	0.005(1)	0	0.001(1)	0
Ti5	0.000	0.3997(2)	0.250	0.008(1)	0.0092(9)	0.006(1)	0	0.000(1)	−0
O1	0.2527(5)	0.6234(5)	0.2421(9)	0.7(1)*					
O2	0.0815(5)	0.1194(5)	0.5940(8)	0.6(1)*					
O3	0.4099(5)	0.4827(5)	0.3212(7)	0.6(1)*					
O4	0.0837(5)	0.2618(5)	0.3238(8)	0.6(1)*					
O5	−0.0794(5)	0.2464(5)	0.6641(8)	0.8(1)*					
O6	−0.0998(5)	0.1233(5)	0.4108(7)	0.3(1)*					
O7	0.2651(5)	0.2435(5)	0.5021(8)	0.7(1)*					
O8	−0.0874(5)	0.3739(5)	0.3987(8)	0.7(1)*					
O9	0.2550(5)	0.3723(4)	0.2501(8)	0.5(1)*					
O10	0.2529(5)	0.4922(6)	0.4986(8)	0.7(1)*					
O11	0.0712(5)	0.5073(5)	0.3440(7)	0.5(1)*					

Note. Site occupancy: [1] 0.81 Zn + 0.15 Ti and 4% vacancy; [2] 0.89 Ti + 0.11 Zn; [3] 0.89 Ti + 0.11 Zn.

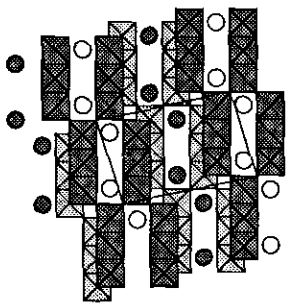

FIG. 18. Ideal representation of the crystal structure of $Ba_2ZnTi_5O_{13}$, apparently isostructural with $Ba_2MgTi_5O_{13}$ and with $K_2Ti_6O_{13}$ (*13*).

zigzag ribbons of $(Ti,Zn)O_6$ octahedra running along c. Each repeating unit in these ribbons comprises a set of three edge-sharing octahedra connected to three other edge-sharing octahedra at a level of one-half unit cell down (and up) along b. The cation positions (Ti,Zn) of the latter octahedra are displaced half an octahedron unit so they are almost directly below (and above) an oxygen apex. No face-sharing of octahedra is found.

This is a relatively open structure. Rectangular open channels of approximate size 3.2 by 2.9 Å can be seen running through the structure parallel to b and passing through the points $(x, y, z) = (0, y, \frac{1}{2})$ and $(\frac{1}{2}, y, \frac{1}{2})$.

Although Zn is more commonly tetrahedrally coordinated, Zn was found to substitute partially for Ti in octahedral sites in this structure. Both the Ti1 and the Ti2 sites have a 5% occupancy by Zn; the Ti3 site, with a 40% occupancy by Zn, is designated TZ. As in the $K_2Ti_6O_{13}$ structure, all Ti–O octahedra are distorted. All Ti and Zn atoms

TABLE IVa

SELECTED BOND DISTANCES (Å) AND ANGLES (°) FOR $Ba_2ZnTi_5O_{13}$

Atoms	Distances	Mult	Atoms	Angle	Mult
Ba–O1	2.829(4)	2	O2–Ti1–O4	105.8(3)	1
Ba–O2	2.697(4)	2	O2–Ti1–O5	81.2(3)	1
Ba–O3	3.063(1)	2	O2–Ti1–O7′	98.7(2)	1
Ba–O4	2.779(4)	2	O2–Ti1–O7″	168.6(3)	1
Ba–O5	3.278(6)	1	O4–Ti1–O5	173.0(3)	1
Ba–O6	3.182(6)	1	O7–Ti1–O7′	151.6(3)	1
Ba–O6	3.143(7)	1	O7–Ti1–O7″	79.3(2)	1
Ti1–O2	1.812(6)	1	O1–Ti2–O2	177.72(3)	1
Ti1–O4	1.800(7)	1	O1–Ti2–O3	94.2(2)	1
Ti1–O5	2.212(6)	1	O1–Ti2–O5	99.1(3)	1
Ti1–O7	2.011(1)	2	O1–Ti2–O6	91.1(2)	2
Ti1–O7″	2.142(6)	1	O3–Ti2–O5	166.7(2)	1
			O6–Ti2–O6′	167.0(4)	1
Ti2–O1	1.884(6)	1			
Ti2–O2	2.111(6)	1			
Ti2–O3	1.886(1)	1			
Ti2–O5	2.050(6)	1	O1–TZ–O4	88.1(3)	1
Ti2–O6	1.962(7)	2	O1–TZ–O5′	100.1(2)	2
			O1–TZ–O6	104.9(3)	1
TZ–O1	1.855(7)	1	O1–TZ–O7	166.9(3)	1
TZ–O4	2.049(6)	1	O4–TZ–O6	167.0(3)	1
TZ–O5	1.990(1)	2	O5–TZ–O5′	156.9(3)	1
TZ–O6	2.082(7)	1			
TZ–O7	2.184(6)	1			

TABLE IVb

SELECTED BOND DISTANCES AND ANGLES FOR $BaZn_2Ti_4O_{11}$

Atoms	Distances	Mult	Atoms	Angle	Mult
Ba–O1	2.835(8)	1	O2–Zn1–O3	109.8(3)	1
Ba–O2	2.874(6)	1	O2–Zn1–O4	109.2(3)	1
Ba–O4	2.814(8)	1	O2–Zn1–O6	106.1(3)	1
Ba–O5	2.942(8)	1	O3–Zn1–O4	105.2(3)	1
Ba–O5	2.998(8)	1	O3–Zn1–O6	112.2(3)	1
Ba–O7	2.926(7)	1	O4–Zn1–O6	107.0(3)	1
Ba–O8	3.101(8)	1			
Ba–O8	3.020(6)	1	O7–Zn2–O11	156.5(3)	1
Ba–O10	2.805(8)	1	O1–Zn2–O8	168.8(3)	1
Ba–O11	2.861(7)	1	O1–Zn5–O10	167.9(3)	1
Ba–O11	2.858(7)	1	O1–Zn2–O5	91.0(3)	1
Ba–O11	3.109(7)	1	O1–Zn2–O7	95.3(3)	1
			O1–Zn2–O10	98.4(3)	1
Zn1–O2	1.957(8)	1	O1–Zn2–O11	103.1(3)	1
Zn1–O3	1.939(7)	1			
Zn1–O4	1.962(7)	1	O1–Ti1–O2	165.8(3)	1
Zn1–O6	1.992(8)	1	O3–Ti1–O10	174.1(3)	1
			O6–Ti1–O9	170.8(3)	1
Zn2–O1	1.980(8)	1	O1–Ti1–O3	89.4(3)	1
Zn2–O5	2.253(7)	1	O1–Ti1–O6	80.5(3)	1
Zn2–O7	2.064(7)	1	O1–Ti1–O9	95.3(3)	1
Zn2–O8	2.356(9)	1	O1–Ti1–O10	91.3(3)	1
Zn2–O10	1.995(8)	1			
Zn2–O11	1.939(7)	1	O3–Ti2–O7	171.9(3)	1
			O5–Ti2–O10	170.2(3)	1
Ti1–O1	2.021(7)	1	O6–Ti2–O9	173.1(3)	1
Ti1–O2	1.972(8)	1	O3–Ti2–O5	81.9(3)	1
Ti1–O3	2.070(8)	1	O3–Ti2–O6	93.3(3)	1
Ti1–O6	2.005(7)	1	O3–Ti2–O9	82.4(3)	1
Ti1–O9	1.920(7)	1	O3–Ti2–O10	90.2(3)	1
Ti1–O10	1.898(8)	1			
			O1–Ti3–O8	171.2(4)	1
Ti2–O3	2.044(7)	1	O4–Ti3–O7	168.7(3)	1
Ti2–O5	2.013(8)	1	O6–Ti3–O9	166.8(3)	1
Ti2–O6	2.047(8)	1	O1–Ti3–O4	97.7(3)	1
Ti2–O7	1.868(7)	1	O1–Ti3–O6	78.4(3)	1
Ti2–O9	1.956(9)	1	O1–Ti3–O7	89.3(3)	1
Ti2–O10	1.998(8)	1	O1–Ti3–O9	93.0(3)	1
Ti4–O2	1.961(8)	2	O2–Ti4–O2	168.2(4)	1
Ti4–O3	2.011(7)	2	O3–Ti4–O5	173.3(3)	2
Ti4–O5	1.910(8)	2	O2–Ti4–O3	81.2(3)	2
			O2–Ti4–O5	92.6(3)	2
Ti5–O4	2.126(7)	2			
Ti5–O8	1.973(8)	2	O4–Ti5–O11	169.6(3)	2
Ti5–O11	1.868(7)	2	O8–Ti5–O8	162.7(4)	1
			O4–Ti5–O4	82.4(4)	1
			O4–Ti5–O8	88.3(3)	1
			O4–Ti5–O8	78.7(3)	1
			O4–Ti5–O11	91.3(3)	1

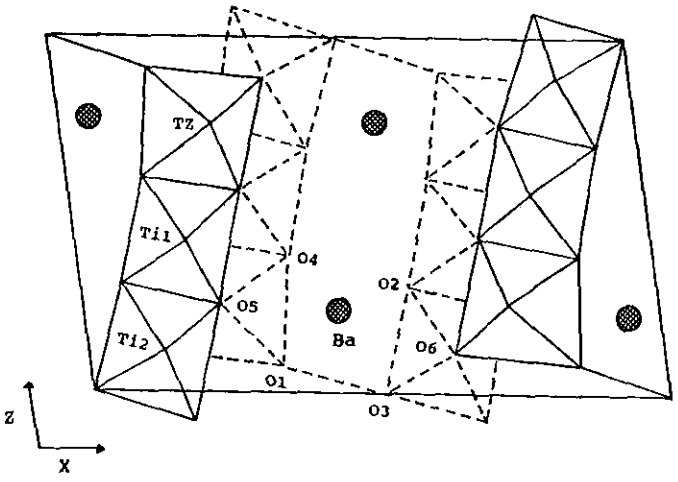

FIG. 19. Representation of the real positions of the Ba and oxygen ions around the Ti and (Ti, Zn) positions in the unit cell of $Ba_2ZnTi_5O_{13}$.

are displaced from the center of the octahedra towards the nearest Ba and open channel sites. This shifting of position probably compensates the less saturated oxygen atoms so as to maintain electroneutrality (*17, 33*).

The Ti–O and Zn–O bond distances in both structures range from 1.80 to 2.22 Å. These distances agree with those found in other titanate and related compounds with 6-coordinate Ti (Table V). For comparison purposes, Table V also lists compounds

TABLE V

SELECTED Ti–O DISTANCES (Å) OF THE $Ti–O_6$ OCTAHEDRA FOUND IN OTHER POLYTITANATES AND RELATED COMPOUNDS—COORDINATION NUMBER (C.N.) OF Ba ARE ALSO GIVEN

	Ti–O		Ba–O	
	Distance	C.N.	C.N.	Ref.
Ba_2TiO_4	1.63,1.64,1.75,1.82	4	8,10	(*38*)
Y_2TiO_5	1.78,1.87,1.91,1.94,1.94, (3.89)	5	—	(*39*)
Fresonite	1.63,2.00,2.00,2.00,2.00, (3.58)	5	—	(*39*)
$BaTi_2O_5$	1.71,1.87,2.00,2.00,2.06,2.47	5 + 1	12	(*17*)
$PbTiO_3$	1.78,1.98,1.98,1.98,1.98,2.38	5 + 1	—	(*40*)
$Na_2Ti_3O_7$	1.71,1.87,1.91,1.94,1.94,2.34	5 + 1	—	(*41*)
$BaTi_4O_9$	1.87 to 2.20	6	10	(*18*)
$K_2Ti_6O_{13}$	1.86,1.95,1.95,1.96,1.98,2.11	6	11	(*33*)
$Ba_2Ti_9O_{20}$	1.82 to 2.26	6	11,12	(*22a*)
$Ba_4Ti_{13}O_{30}$	1.87,1.87,1.95,1.95,2.09,2.09	6	11	(*21*)
$Ba_6Ti_{17}O_{40}$	1.83,1.87,1.88,1.90,1.93,1.99	6	12	(*20*)
$BaTi_5O_{11}$	1.77,1.94,1.94,1.94,2.04,2.07	6	12	(*42*)
$Ba_4Zn_2Ti_{10}O_{26}$	1.88,1.88,1.96,1.96,2.05,2.11	6	11	
$BaZn_2Ti_4O_{11}$	1.90,1.92,1.97,2.00,2.02,2.07	6	12	
$Ba_4Ti_{10}Al_2O_{27}$	1.86,1.91,1.93,1.07,2.02,2.11	6	11,12	(*32*)

having 4-, 5-, and (5 + 1)-coordinate Ti. While Ti in Y_2TiO_3 is clearly 5-coordinate, Ti in $BaTi_2O_5$, $PbTiO_3$, and $Na_2Ti_3O_7$ can be considered to be (5 + 1)-coordinate. The range of Ti–O bond distances appears to be smaller in the compounds with 6-coordinate Ti than those with (5 + 1)-coordinate Ti (e.g., 1.71 to 2.4 Å in $BaTi_2O_5$).

Figure 20 shows the coordination environment around Ba. Instead of 12 nearest-neighbor oxygens as in a close-packed structure, Ba has only 11 nearest-neighbor oxygens. This polyhedron can be described as a tricapped quadrilateral prism with the Ba–O distances ranging from 2.7 to 3.2 Å. Ba occupies a position displaced from the center of the cage.

4.2. Crystal Structure of "$BaZn_2Ti_4O_{11}$"

As mentioned earlier, the formula of this compound was first reported to be $Ba_3Zn_7Ti_{13}O_{34}$ by Gornikov *et al.* (*2*), who formed the compound by adding ZnO to $BaTi_4O_9$. Ceramic specimens on the join $BaTiO_4$–$BaZn_2Ti_4O_{11}$ always contain a small amount of the hollandite phase in the X-ray diffraction powder pattern and have a low Q at microwave frequencies. For this reason, particular attention was paid to the refinement of atomic occupations with the assumption that the real composition of the phase might be low in TiO_2. The relatively large R factor may not justify attempting to refine population parameters and amount of disorder between Zn and Ti atoms in the octahedral sites; nevertheless, such refinements were carried out in an attempt to explain the observed X-ray powder diffraction data and physical properties. Present results from single crystal determination indicate the formula to be between $BaZn_2Ti_4O_{11}$ and $BaZn_{2.03}Ti_{3.93}O_{10.89}$. The R values of these refinements are very close (i.e. from 0.0644 to 0.0640 for R). The best R value appears to occur for the choice of the formula $BaZn_{2.03}Ti_{3.93}O_{10.89}$. In this case, in order to maintain the electroneutrality of this phase, it was found necessary to assume a small oxygen deficiency. Site vacancies could be assigned to positions of the oxygen ions coordinating the "octahedral" Zn2 ions: O1(5%), O10(4%), and O11(2%). Such a refinement resulted in lowering abnormally large temperature factors. However, since the chemical formula cannot be determined in a more absolute manner, the stoichiometric formula "$BaZn_2Ti_4O_{11}$" will be used throughout this report, even though the data shown in Tables IIIa and b are derived from $BaZn_{2.03}Ti_{3.93}O_{10.89}$.

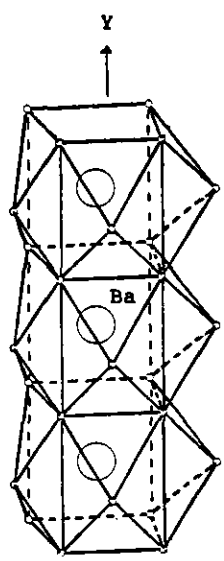

FIG. 20. Polyhedra arrangement surrounding the Ba atoms in $Ba_2ZnTi_5O_{13}$ illustrating the infinite chain of tricappled quadralateral prisms parallel to y.

The overall structure consists of a three dimensional network of distorted, edge-sharing and corner-sharing octahedra with Zn filling some tetrahedral intersticies. Ti atoms were found to occupy only octahedral positions; Zn atoms were found to occupy both tetrahedral and octahedral intersticies. Figure 21 shows the arrangement of idealized TiO_6 and ZnO_6 octahedra and ZnO_4 tetrahedra in each level $y = n/6$ (n = 1, 2, 3, . . . , 6) viewed along the b axis. There is a substantially different arrangement at

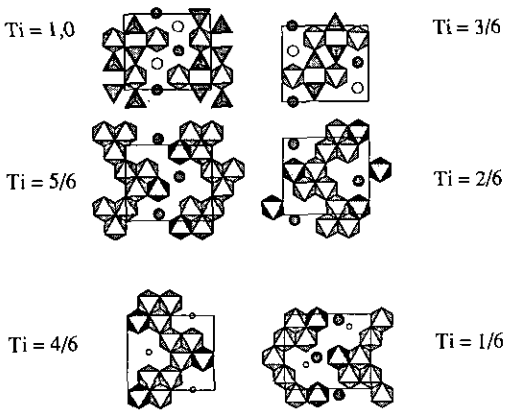

FIG. 21. Ideal representations of the crystal structure of $BaZn_2Ti_4O_{11}$ at the six (Ti, Zn) levels of the unit cell. Dark triangles represent ZnO_4 polyhedra pointing up and down and dark octahedra represent the "ZnO_6" octahedra.

each level. Each unit cell contains a total of 8 ZnO_4, 8 ZnO_6, and 32 TiO_6 units. No ZnO_4 or ZnO_6 units share polyhedral corners or edges. The ZnO_4 tetrahedra are near the $y = 0$ and $y = \frac{1}{2}$ levels of the unit cell. There is no face-sharing of octahedra within or between layers.

Substitution of Zn for Ti on octahedral sites was again considered. The Zn1 atom is in a tetrahedral site that probably never contains Ti; Zn2 and all Ti atoms are in octahedral sites and might substitute for one another within certain limits. The least squares refinement procedure was therefore pushed beyond its crystallographically reasonable limits while particular attention was paid to such crystal chemical principles and the observed physical properties. For example, 11% each of the Ti1 and Ti2 atoms could be replaced by Zn, and the best R values appear to occur when it is assumed that $\approx$11% of the Zn2 atoms are replaced by Ti and 4% of the Zn2 sites are left vacant (the stoichiometric composition requires 22% of Zn2 to be replaced by Ti). From Table IVb, it is seen that the bond lengths in the ZnO_4 tetrahedron are relatively small, ranging from 1.939 to 1.992 Å, in agreement with the Zn–O distances found in other compounds, such as Zn_2SiO_4 (1.941 to 1.987 Å) (*43*). Bond lengths in the octahedra vary according to which cations occupy the sites. The Zn–O distances range from 1.939 to 2.356 Å, whereas the Ti–O distances range from 1.868 to 2.126 Å. Most of these TiO_6 and ZnO_6 cages have low symmetry except for Ti4 and Ti5 which are on a 2-fold axis. From the bond lengths and bond angles given in Table IVb, the distortion from ideal polyhedra is clear. For example, the axial O–Ti–O angles deviate significantly from 180°. For Zn these angles range from 156° to 169°, and for Ti they range from 166° to 174°. It appears that the ZnO_6 octahedra are relatively more distorted than the Ti ones.

The Ba atom has a close-packed (C.N. = 12) environment. The twelve Ba–O distances vary between 2.834(8) and 3.109(7) Å, which is within the range found in other barium titanate structures (*17, 20, 22a, 32, 42*).

References

1. T. NEGAS, G. YEAGER, S. BELL, AND R. AMREN; *in* "Chemistry of Electronic Ceramic Materials" (P. K. Davies and R. S. Roth, Eds.), Proc. of The Int. Conf. Jackson, WY, Aug. 17–22, 1990, SP804, pp.21–37, National Institute of Standards and Technology, Gaithersburg, MD (1991).
2. YU. I. GORNIKOV, Z. YA MAKROVA, A. G. BELOUS, L. G. GAVRILOVA, V. M. PASHKOV, AND V. P. CHALYI, *Ukr. Khim. Zh.* **50**(12), 1243–45 (1984); Engl. trans. *Sov. Prog. Chem.* **50**,(12), 11–12 (1984).
3. U. SPITSBERGEN, *Acta Crystallogr.* **13**, 197–198 (1960).
4. M. D. HILL AND R. S. ROTH, to be published.
5. F. H. DULIN AND D. E. RASE, *J. Am. Ceram. Soc.* **43**(3), 125–131 (1960).
6. "Phase Diagrams for Ceramists," Vols. 1–6, Am. Ceram. Soc., Columbus, OH (1964–1987).
7. "Standard X-Ray Diffraction Powder Patterns," NBS Monograph 25 12m, p. 37 (1975).
8. D. E. RASE AND R. ROY, *J. Am. Ceram. Soc.* **38**(3), 102–113 (1955).
9. T. NEGAS, R. S. ROTH, H. S. PARKER, AND D. B. MINOR, *J. Solid State Chem.* **9**, 297–307 (1974).
10. J. J. RITTER, R. S. ROTH, AND J. E. BLENDELL, *J. Am. Ceram. Soc.* **62**(2), 155–163 (1986).

11. H. M. O'Bryan, Jr., and J. Thomson, Jr., *J. Am. Ceram. Soc.* **57**,(12), 522–526 (1974).
12. K. W. Kirby and B. A. Wechsler, *J. Am. Ceram. Soc.* **74**(8), 1841–1847 (1991).
13. G. H. Jonker and W. Kwestroo, *J. Am. Ceram. Soc.* **41**(10), 390–394 (1958).
14. R. S. Roth, J. J. Ritter, H. S. Parker, and D. B. Minor, *J. Am. Ceram. Soc.* **69**(12), 858–862 (1986).
15. M. C. Morris, H. F. McMurdie, E. H. Evans, B. Paretzkin, H. S. Parker, N. P. Pyrros, W. Wong-Ng, D. M. Gladhill, and C. R. Hubbard, "Standard X-Ray Diffraction Powder Patterns," NBS Monograph 25, Sects. 20, 21 (1984–1985).
16. F. W. Harrison, *Acta Crystallogr.* **9**, 495–500 (1956).
17. E. Tillmanns, *Acta Crystallogr. Sect. B* **30**, 2894–2896 (1974).
18. K. Lukaszewicz, *Rocz. Chem.* **31**, 1111–1122 (1957).
19. W. Hofmeister, E. Tillmans, and W. H. Baur, *Acta Crystallogr.*, to appear.
20. E. Tillmans and W. H. Baur, *Acta Crystallogr. Sect. B* **26**(11), 1645–1655 (1970).
21. E. Tillmans, *Inorg. Nucl. Chem. Lett.* **7**(12), 1169–1171 (1971) and *Cryst. Struct. Commun.* **11**, 2087–2092 (1982).
22. (a) E. Tillmans, W. Hofmeister, and W. H. Baur, *J. Am. Ceram. Soc.* **66**(4), 268–271 (1983); (b) G. D. Fallon and B. M. Gatehouse, *J. Solid State Chem.* **49**, 56–64 (1983).
23. E. Tillmans, *Acta Crystallogr. Sect. B* **25**(8), 1444–1452 (1969).
24. E. Tillmans, *Cryst. Struct. Commun.* **1**, 1–4, (1972).
25. P. K. Davies and R. S. Roth, *J. Solid State Chem.* **71**, 503–512 (1987).
26. P. K. Davies and R. S. Roth, *J. Solid State Chem.* **71**, 490–502 (1987).
27. J. G. Allpress and R. S. Roth, *J. Solid State Chem.* **3**, 209–216
28. R. S. Roth, *Prog. Solid State Chem.* **13**(2), 168 (Fig. 17) (1980).
29. M. M. Hedges, M. J. Bannister, and M. S. J. Gani, *J. Am. Ceram. Soc.* **74**(9), 2318–2320 (1991).
30. B. M. Gatehouse, G. D. Fallen, and R. S. Roth, to be published.
31. R. S. Roth, W. S. Brower, M. Austin, and M. Koobin, NBSIR 81-2441., Nat. Meas. Lab., Office of Meas. for Nuclear Tech. Annual Report pp.42–48 (1981).
32. J. Schmachtel and H. K. Müller-Buschbaum, *Z. Anorg. Allg. Chem.* **472**, 89–94 (1981).
33. H. Cid-Dresdner and M. J. Buerger, *Z. Kristallogr.* **117**, 411–430 (1962).
34. J. M. Millet, R. S. Roth, L. D. Ettlinger, and H. S. Parker, *J. Solid State Chem.* **67**, 259–270 (1987).
35. R. S. Roth, L. D. Ettlinger, and H. S. Parker, *J. Solid State Chem.* **68**, 330–339 (1987).
36. "CAD4 Operations Manual," Enraf–Nonius, Delft (1977).
37. "MOLEN, An Interactive Structure Solution Procedure," Enraf–Nonius, Delft (1990).
38. J. A. Bland, *Acta Crystallogr.* **14**, 875 (1961).
39. W. G. Mumme and A. D. Wadsley, *Acta Crystallogr. Sect. B* **24**, 1327 (1968).
40. G. Shirane, R. Pepinsky, and B. C. Frazer, *Acta Crystallogr.* **9**, 131 (1956).
41. S. Anderson and A. D. Wadsley, *Acta Crystallogr.* **14**, 1245 (1961).
42. J. Schmachtel, *Acta Crystallogr. Sect. B* **25**, 1444 (1969).
43. C. Hang, M. A. Simonov, and N. V. Belov, *Sov. Phys. Crystallogr.* **15**(3), 387 (1970).